



HAL
open science

Structural characterization of HC-Pro, a plant virus multifunctional protein.

Célia Plisson, M. Drucker, S. Blanc, S. German-Retana, O. Le Gall, Daniel Thomas, Patrick Bron

► **To cite this version:**

Célia Plisson, M. Drucker, S. Blanc, S. German-Retana, O. Le Gall, et al.. Structural characterization of HC-Pro, a plant virus multifunctional protein.. *Journal of Biological Chemistry*, 2003, 278 (26), pp.23761. 10.1074/jbc.M302512200 . hal-00108282

HAL Id: hal-00108282

<https://hal.science/hal-00108282v1>

Submitted on 31 May 2020

HAL is a multi-disciplinary open access archive for the deposit and dissemination of scientific research documents, whether they are published or not. The documents may come from teaching and research institutions in France or abroad, or from public or private research centers.

L'archive ouverte pluridisciplinaire **HAL**, est destinée au dépôt et à la diffusion de documents scientifiques de niveau recherche, publiés ou non, émanant des établissements d'enseignement et de recherche français ou étrangers, des laboratoires publics ou privés.



Distributed under a Creative Commons Attribution - NonCommercial 4.0 International License

Structural Characterization of HC-Pro, a Plant Virus Multifunctional Protein*

Received for publication, March 12, 2003, and in revised form, April 1, 2003
Published, JBC Papers in Press, April 8, 2003, DOI 10.1074/jbc.M302512200

Célia Plisson‡§, Martin Drucker§¶, Stéphane Blanc¶||, Sylvie German-Retana**, Olivier Le Gall**, Daniel Thomas‡, and Patrick Bron‡ ††

From the ‡Université Rennes I, Unité Mixte de Recherche 6026 CNRS, Campus de Beaulieu, Rennes 35042,

¶Station de Recherches de Pathologie Comparée Unité Mixte de Recherche 5087 Institut National de la Recherche

Agronomique-CNRS-Université Montpellier II, Saint-Christol-lez-Alès 30380, and **Institut National de la Recherche

Agronomique, Virologie, Institut de Biologie Végétale Moléculaire, BP 81, Villenave d'Ornon Cedex 33883, France

The helper component proteinase (HC-Pro) is a key protein encoded by plant viruses of the genus *Potyvirus*. HC-Pro is involved in different steps of the viral cycle, aphid transmission, replication, and virus cell-to-cell and systemic movement and is a suppressor of post-transcriptional gene silencing. Structural knowledge of HC-Pro is required to better understand its multiple functions. To this aim, we purified His-tagged wild-type HC-Pro and a N-terminal deletion mutant (Δ HC-Pro) from plants infected with recombinant potyviruses. Biochemical analysis of the recombinant proteins confirmed that HC-Pro is a dimer in solution, that the N terminus is not essential for self-interaction, and that a large C-terminal domain is highly resistant to proteolysis. Two-dimensional crystals of the recombinant proteins were successfully grown on Ni²⁺-chelating lipid monolayers. Comparison of projection maps of negatively stained crystals revealed that HC-Pro is composed of two domains separated by a flexible constriction. Cryo-electron crystallography of Δ HC-Pro allowed us to calculate a projection map at 9-Å resolution. Our data from electron microscopy, biochemical analysis, and secondary structure predictions lead us to suggest a model for structure/function relationships in the HC-Pro protein.

The genus *Potyvirus* is one of the largest genera of plant RNA viruses. The potyvirus genome encodes a single polypeptide that is processed by three viral proteinases to release all viral proteins needed for the infection cycle. One of these proteins is HC-Pro (helper component proteinase). HC-Pro fulfills many functions in the viral cycle (reviewed in Refs. 1 and 2). It was first recognized as an indispensable helper factor for virus host-to-host transmission by aphid vectors (3). Later, a protease activity was found acting in *cis* on its own C terminus to release it from the precursor polyprotein (4). Subsequent research identified further functions of HC-Pro; it is a general enhancer of infectivity and genome amplification and is indispensable for cell-to-cell and systemic movement in the plant

(5). More recently, it has been identified as a suppressor of post-transcriptional gene silencing (PTGS)¹ and virus-induced gene silencing (6).

Mutagenesis studies and sequence alignments suggest that HC-Pro can be schematically divided into three regions: an N-terminal region essential for the transmission process, a C-terminal region harboring the proteinase activity, and a central region implicated in all other functions (see Fig. 1). This view is probably too simplistic, and many functions most likely overlap in the HC-Pro sequence as described below.

The transmission function involves two conserved motifs. One is the N-terminal KITC motif (amino acid (AA) 52–55; numbering according to HC-Pro from *Lettuce mosaic virus* (LMV)) that is involved in binding to the aphid vector's stylets (7). The other is the C-terminal PTK motif (AA 310–312) that probably contributes to binding of HC-Pro to the viral capsid protein's N-terminal DAG motif (8, 9). The DAG motif-PTK motif interaction is essential for transmission, but a second HC-Pro binding motif might exist in the capsid protein, perhaps with different functions (10). The N-terminal ~100 AA of HC-Pro seem to be only involved in the transmission process, because viral mutants deleted of this region are fully infectious (11).

The proteinase domain has been mapped to the C-terminal 155 AA and characterized as a cysteine protease-like activity with Cys³⁴⁴ and His⁴¹⁷ residues in the active site (4). This region might also overlap with a cell-to-cell movement domain, as in *Bean common mosaic necrosis virus* HC-Pro, a C-terminal deletion of 87 and 293 AA, respectively, partially or totally abolished cell-to-cell movement of heterogeneously expressed protein in microinjection studies (12).

The central region of HC-Pro (AA 100–300) is generally assumed to be important in genome amplification (IGN motif, AA 260–262), synergism with other viruses, and systemic movement within the host plant (CC/SC motif, AA 292–295) (5, 13). Two domains (A and B) spanning the entire central region were described as non-specifically binding nucleic acids with a preference for single-stranded RNA. The B domain shares homology with ribonucleoproteins (14, 15).

Recently, HC-Pro has been recognized as a suppressor of PTGS and virus-induced gene silencing (for reviews see Refs. 16 and 17). PTGS, virus-induced gene silencing, and other RNA silencing phenomena are ancient defense mechanisms found in several eukaryotes and might constitute an alternative im-

* The work was supported in part by a grant from the Ministère de l'Enseignement Supérieur et de la Recherche (to C. P.). The costs of publication of this article were defrayed in part by the payment of page charges. This article must therefore be hereby marked "advertisement" in accordance with 18 U.S.C. Section 1734 solely to indicate this fact.

§ Contributed equally to this work.

¶ To whom correspondence may be addressed. Tel.: 33-0-4-66-78-37-15; Fax: 33-0-4-66-52-46-99; E-mail: blanc@ensam.inra.fr.

†† To whom correspondence may be addressed. Tel.: 33-0-2-23-23-69-82; Fax: 33-0-2-23-23-50-48; E-mail: patrick.bron@univ-rennes1.fr.

¹ The abbreviations used are: PTGS, post-transcriptional gene silencing; AA, amino acid(s); LMV, *Lettuce mosaic virus*; 2D, two-dimensional; Ni-NTA, nickel-nitrilotriacetic acid; DOGS, dioctadecylamidoglycospermine.

mune system where short interfering RNAs mediate specific degradation of aberrant RNA such as viral RNA. In plants, the phloem distributes an unidentified silencing signal throughout the plant, and as a result the whole plant suppresses expression of the concerned gene. Many plant viruses have evolved counterstrategies to knock out PTGS and encode PTGS suppressors such as HC-Pro. HC-Pro does not interfere with the mobile silencing signal but inhibits accumulation of short interfering RNA through an unknown mechanism (18). The central region of HC-Pro is implicated in suppressor activity and overlaps with the region identified for genome amplification and viral movement (19).

Although many functions of HC-Pro have been well characterized by mutagenesis studies, little is known about the molecular mechanisms involved and the links between the various activities. Size exclusion chromatography suggests that the functional HC-Pro in transmission is a dimer or trimer (3, 20). Yeast two-hybrid experiments to test for HC-Pro self-interaction yielded somewhat confusing results. One group reported that only the N terminus is involved in HC-Pro self-interaction (21), whereas another group identified interaction sites in both the N terminus and the C-terminal proteinase domain (22).

Knowledge of the structure of HC-Pro will greatly contribute to understand its multifaceted functions and how structural domains are organized to fulfill them in concert or independently. To this aim, we analyzed the structure of HC-Pro of LMV by biochemistry and electron microscopy. We fused a histidine tag (His tag) to the N terminus of both wild-type HC-Pro and a 99-AA N-terminal deletion mutant (Δ HC-Pro) in the viral context. This strategy allowed purification of the recombinant proteins from infected plants and provided a convenient means for targeting HC-Pro to nickel-chelating lipid interfaces for electron microscopy of two-dimensional (2D) crystals (for a review see Ref. 23). Biochemical analysis confirmed the dimeric nature of soluble HC-Pro and provided information on regions responsible for dimerization. Furthermore, 2D crystals of the two recombinant proteins were obtained and suitable for structural analysis by electron microscopy and image processing. We present here projection maps of the two negatively stained recombinant proteins and a projection structure of frozen-hydrated Δ HC-Pro at 9-Å resolution. Finally we discuss relationships between HC-Pro's structural organization and biological functions.

MATERIALS AND METHODS

Construction of Recombinant Viruses—Recombinant LMV-E mutants were obtained by insertion in the plasmid p70SLMVE of a His₆ tag fused to the N terminus of either wild-type HC-Pro or of a deleted form (99 AA) of HC-Pro. p70SLMVE contains an infectious, full-length cDNA copy of LMV-E RNA, under the control of the enhanced cauliflower mosaic virus (CaMV) 35S promoter and the NOS terminator (24). The resulting recombinants were designated *his*HC-Pro and *his* Δ HC-Pro. Briefly, we introduced a *Sma*I site (CCCGGG) at the level of the *Aat*II site (nucleotides 1418–1423) that corresponds to the second and third codons of the HC-Pro sequence. The resulting plasmid pLMV-E-*Sma*HC contains a new *Sma*I site surrounded by two *Aat*II sites at the beginning of the HC-Pro coding sequence. Finally, the sequence CAT-CACCACCACCACCAT encoding six histidines was inserted as a double-stranded oligonucleotide in the newly created *Sma*I site. This yielded plasmid pLMV-E-*his*HC-Pro where the viral protein P1 cleavage site necessary for liberation of HC-Pro from the polyprotein precursor is conserved. The AA sequence of the N terminus of *his*HC-Pro is SDVpgduARN (inserted AA in italics). A similar strategy was used to clone pLMV-E-*his* Δ HC-Pro where the HC-Pro sequence was deleted of AA 4–102 in LMV-E-*Sma*HC and where the histidine-tagged deleted HC-Pro has the N-terminal AA, SDVpgKQV. Sequencing of recombinant LMV *his* Δ HC-Pro RNA amplified by reverse-transcriptase PCR showed that the HC-Pro sequence of infectious *his* Δ HC-Pro virus recombinant contained a Gly to Ala substitution resulting in a Gly to Arg change of AA 183 (AA 285 in wild-type HC-Pro) without any effect on infectivity of the virus.

Purification of HC-Pro and Δ HC-Pro—Young pea (*Pisum sativum* L.) plants were inoculated with the recombinant viruses as described (25). Pea leaves harboring disease symptoms characteristic of either recombinant virus were harvested 2 to 3 weeks after inoculation. They were homogenized in a blender together with 2 volumes of ST Buffer (100 mM Tris, pH 8.0, 20 mM Mg₂SO₄, 0.5 mM EGTA) supplemented with 500 mM NaCl, 0.2% Na₂SO₃, and 0.1% polyvinylpyrrolidone (PVP). The brei was filtered through four layers of cheesecloth and one layer of miracloth (Calbiochem) and centrifuged for 60 min at 100,000 \times g. To concentrate the supernatant containing HC-Pro, differential precipitation with (NH₄)₂SO₄ (20–40% for *his*HC-Pro and 20–50% for *his* Δ HC-Pro) was carried out, and the HC-Pro-containing fraction was resuspended in ST Buffer plus 0.5 M NaCl and stored at -70 °C.

Several preparations were thawed and centrifuged for 5 min at 5,000 \times g, the supernatant was mixed with 1 ml of Ni-NTA resin (Qiagen), and 10% methanol was added. After 30 min of incubation on ice, the resin was rinsed two times for 30 min in a batch procedure with 50 ml of ST Buffer plus 500 mM NaCl and 10% methanol, followed by two washes with 50 ml of ST Buffer plus 100 mM NaCl. Then the resin was applied on a column and eluted with 5 ml of ST Buffer plus 100 mM NaCl and 500 mM imidazole. The elute was precipitated with 60% (NH₄)₂SO₄, resuspended in ST Buffer plus 1 M NaCl (2 M for *his* Δ HC-Pro), and loaded on a phenyl-agarose column (Sigma) operated at room temperature. The column was washed with five volumes of the same buffer and eluted with five volumes of ST Buffer. The eluate was precipitated with 80% (NH₄)₂SO₄, the pellet was washed two times with 80% (NH₄)₂SO₄, and the protein was stored in 80% (NH₄)₂SO₄ at 4 °C until use.

Size Exclusion Chromatography—Purified *his*HC-Pro or *his* Δ HC-Pro was centrifuged at 10,000 \times g for 10 min before size exclusion chromatography with Ultrogel AcA 34 resin in a XK70 column (Amersham Biosciences). The running buffer was ST Buffer plus 100 mM NaCl. Gel runs were carried out on an ÄKTA Prime system (Amersham Biosciences) at 4 °C with a flow rate of 0.1 ml/min and monitoring the absorbance at 280 nm. The column was calibrated with a kit for molecular masses of 29,000–700,000 Da (Sigma).

Chemical Cross-linking—5 μ l of protein solution was incubated with 1 μ l of 12.5 mg/ml 1,8-bis-maleimidotriethyleneglycol (Pierce) solution in *N,N*-dimethylformamide or with 1 μ l of 0.1% glutaraldehyde for 5–60 min on ice. The reaction was quenched with 4 \times Laemmli buffer, the samples were boiled for 5 min, and the proteins were analyzed by SDS-PAGE. *N,N*-Dimethylformamide alone had no effect on the oligomerization state of the proteins.

Limited Proteolysis—Solutions of *his*HC-Pro or *his* Δ HC-Pro in ST Buffer plus 100 mM NaCl were incubated for the times indicated with 1.0 \times trypsin solution (Invitrogen) at 37 °C. Adding 4 \times Laemmli buffer and boiling of the samples for 5 min stopped the reaction before analysis of the proteins by SDS-PAGE. For N-terminal sequencing of the 32-kDa proteolysis product, we employed identical conditions, except that 0.5 μ g of sequencing grade trypsin (Promega) was used for 1 μ g of protein.

N-terminal Sequencing—The proteolysis products were separated by SDS-PAGE and transferred to a polyvinylidene difluoride membrane. The 32-kDa band was identified by Ponceau S staining, cut off, and extensively washed with water. N-terminal sequencing was carried out by Edman sequencing.

2D Crystallization—We obtained 2D crystals of *his*HC-Pro and *his* Δ HC-Pro by the following method. A lipid mixture was made of the ligand lipid, DOGS-Ni-NTA, and the diluting lipid, dioleoyl phosphatidylcholine, at a molar ratio of 1:1 in chloroform/methanol (9/1, v/v) and a final concentration of 0.5 mg/ml. Lipids were purchased from Avanti Polar Lipids. 0.5 μ l of the lipid mixture was spread on the surface of a drop in a Teflon well (54 μ l) containing Buffer A (20 mM Tris-HCl, pH 8.0, 200 mM MgCl₂). The Teflon wells used in these experiments were designed for 2D crystallization of membrane proteins on lipid layers (26). Each well was connected to a side hole allowing injection of the protein solution. After overnight incubation at room temperature in a humid chamber, 3 μ l of protein solution was injected below the lipid layer, and the solution was gently stirred without perturbing the surface lipid layer. Crystallization samples were incubated at room temperature in a humid chamber. After 24 to 48 h, a holey carbon grid was deposited on the surface of the drop, and the transferred sample was negatively stained with 1% uranyl acetate for 30 s and then carbon-coated (27). For observation of frozen-hydrated 2D crystals of *his* Δ HC-Pro, plane carbon-coated gold grids were placed on top of the crystallization wells and left in contact with the interface for 2 h. Excess buffer was blotted with filter paper, and the grids were frozen rapidly in liquid ethane and stored in liquid nitrogen (28).

Electron Microscopy and Image Analysis—Specimens were examined

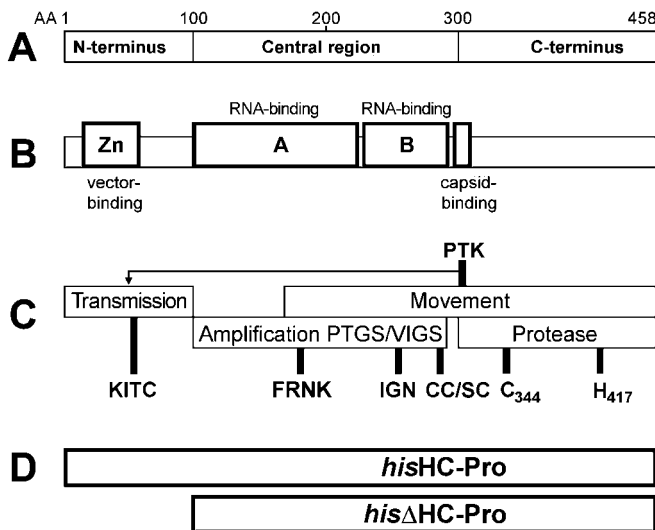


FIG. 1. Functional regions of HC-Pro and recombinant HC-Pro used in this study. *A*, HC-Pro can be nominally divided into three regions. Numbering of AA is according to the HC-Pro sequence of LMV-E. *B*, location of the putative vector-binding, RNA-binding, and viral capsid-binding regions in the HC-Pro sequence. *Zn*, putative zinc finger; *A* and *B*, RNA-binding domains. *C*, biological functions of different HC-Pro regions and position of conserved motifs. The arrow indicates that the PTK motif is also involved in transmission. *D*, recombinant HC-Pro mutants used in this study. A His₆ tag was fused adjacent of the N-terminal cleavage site of full-length (*hisHC-Pro*) or deleted (AA 4–102) HC-Pro (*hisΔHC-Pro*).

in a Philips CM12 electron microscope equipped with a LaB6 filament, operating at 120 kV. Suitable 2D crystals were imaged on Eastman Kodak Co. SO-163 film at a precalibrated electron optical magnification of $\times 43,750$, using low dose techniques. Frozen-hydrated specimens were imaged using a Gatan 626 cryo-holder. Micrographs were developed for 12 min at 20 °C.

Micrographs selected by optical diffraction were digitized at 15- μ m pixel size for negatively stained specimens and 10 μ m for frozen-hydrated specimens with a HI-SCAN (Eurocore). Images were processed using the MRC image processing programs (29). Briefly, the Fourier transform of each image was calculated, and the cell parameters were determined. The images were corrected for distortions of the crystal lattice by cross-correlation Fourier analysis and re-interpolation of the image (30, 31). Amplitudes and phases were extracted using MMBBOXA. The defocus and astigmatism values were first determined by CTFFIND and subsequently refined during the merging procedure. Images were corrected for the contrast transfer function using CTFAPPLY. Phase relationships between Fourier components of each crystal were examined with the program ALLSPACE (32), and the space group was determined. Comparison of the internal phase residual in all 17 space groups revealed *p4* symmetry. The common origin was refined, and the contrast transfer function-corrected data was merged. The phases were rounded to either 0 or 180°, as the projection structure was centro-symmetric in this plane group. With the amplitudes and phases obtained after image processing, Fourier projection maps were calculated using the CCP4 program package (33).

Sequence Analysis and Predictive Methods—Predictions of secondary structure of *hisHC-Pro* and *hisΔHC-Pro* were computed using the programs PHD (34, 35), Hnn (35), nnpredict (36, 37), Jpred (38, 39), and SOPM_A (40).

SDS-PAGE, Western Blot, and Antibodies—SDS-PAGE was carried out using standard methods with 12% polyacrylamide gels. Gels were stained with Coomassie Blue or transferred to nitrocellulose using a semi-dry blotting apparatus. Bound antibodies were detected with the nitro blue tetrazolium/5-bromo-4-chloro-3-indolyl phosphate (NBT/BCIP) color reaction or by enhanced chemiluminescence (Pierce). For detection of HC-Pro a rabbit polyclonal antiserum was used, and for detection of His tags a commercial mouse monoclonal antibody (Eurogentec) was used.

RESULTS

Expression of Functional Recombinant HC-Pro—Two LMV recombinants were constructed (Fig. 1), where a His tag was

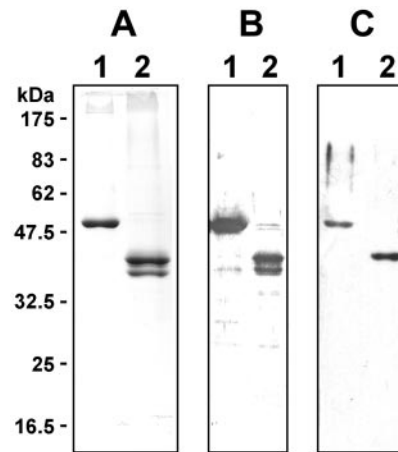


FIG. 2. Purification of *hisHC-Pro* and *hisΔHC-Pro*. *A*, Coomassie Blue-stained SDS-PAGE gel of purified *hisHC-Pro* and *hisΔHC-Pro*. *B*, Western blot of purified *hisHC-Pro* and *hisΔHC-Pro* probed with a polyclonal HC-Pro antiserum. *C*, Western blot of purified *hisHC-Pro* and *hisΔHC-Pro* probed with a monoclonal His₆ antibody. Lanes 1 correspond to *hisHC-Pro*, and lanes 2 correspond to *hisΔHC-Pro*. Molecular mass markers are indicated at the left.

inserted upstream of the wild-type HC-Pro sequence (*hisHC-Pro*) or of a mutant deleted of AA 4 to 102 (*hisΔHC-Pro*). The recombinant viruses were used to inoculate young pea (*P. sativum* L.) plants. The two LMV mutants were fully infectious, and plants displayed typical disease symptoms 8 to 10 days after inoculation. *hisHC-Pro* and *hisΔHC-Pro* were purified from infected plants as described under “Materials and Methods.” Fig. 2 shows that *hisHC-Pro* displayed a single band of the expected size of 53 kDa in SDS-PAGE whereas *hisΔHC-Pro* migrated consistently as a double band, one corresponding to the calculated mass of 41 kDa, the other being about 2 kDa smaller. In Western blots probed with a anti-His₆ antibody, only the upper band was revealed, suggesting that *hisΔHC-Pro* is cleaved *in planta* at its N terminus. In aphid transmission tests, *hisHC-Pro* was active, whereas *hisΔHC-Pro* was inactive (data not shown). In protein overlay assays, the two HC-Pro variants interacted with the coat protein from several potyvirus species, in accordance with previous reports on HC-Pro from other potyviruses (8, 9), further confirming structural integrity of the purified proteins.

The N Terminus of HC-Pro Is Not Essential for Oligomerization—We subjected *hisHC-Pro* and *hisΔHC-Pro* to size exclusion chromatography to determine their native oligomerization state (Fig. 3A). *hisHC-Pro* eluted at a volume equivalent to 138 ± 35 kDa (four independent experiments). This corresponds to a dimer or trimer, as already reported for HC-Pro from other potyviruses (3, 20). Surprisingly, *hisΔHC-Pro* eluted at a volume equivalent to 96 ± 11 kDa (three independent experiments), also suggestive of a dimer or trimer. This indicates that the N terminus of HC-Pro is not essential for oligomerization. The results imply that soluble *hisHC-Pro* as well as *hisΔHC-Pro* are either globular trimers or non-globular dimers. To determine more precisely the oligomeric state of soluble *hisHC-Pro* and *hisΔHC-Pro*, we subjected both proteins to chemical cross-linking with an Src homology-reactive compound, 1,8-bis-maleimidotriethyleneglycol. Fig. 3B shows that, after adding the cross-linker compound, both *hisHC-Pro* and *hisΔHC-Pro* migrated in SDS-PAGE as dimers, in addition to monomer forms. Occasionally, we also observed tetramers and higher oligomers. Experiments with lysine-reactive compounds and glutaraldehyde as cross-linking agents gave similar results (data not shown). In the case of *hisΔHC-Pro*, only one band corresponding to a dimer was visible instead of the three ex-

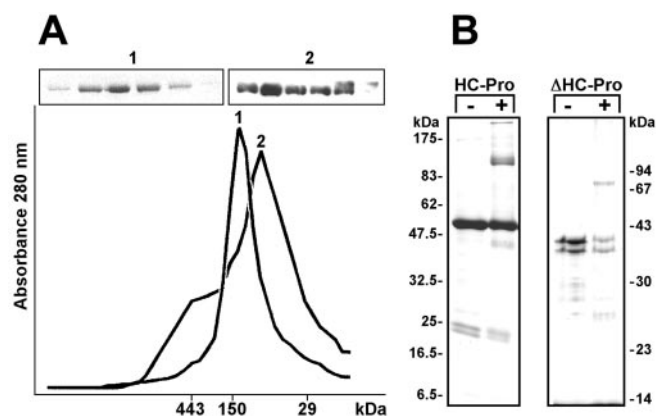


FIG. 3. *hisHC-Pro* and *hisΔHC-Pro* are dimers. *A*, elution profiles of *hisHC-Pro* (1) and *hisΔHC-Pro* (2) in size exclusion chromatography. The elution peak of *hisHC-Pro* corresponds to a molecular mass of 138 kDa, and that of Δ HC-Pro corresponds to a mass of 96 kDa. The insets show a Coomassie Blue-stained SDS-PAGE gel of the peak fractions containing *hisHC-Pro* (1) and a Western blot of the fractions containing *hisΔHC-Pro* (2). Elution peaks of molecular mass markers are indicated on the x-axis. *B*, chemical cross-linking with 1,8-bis-maleimidotriethyl-ene glycol gives rise to a reaction product corresponding to a dimer of *hisHC-Pro* (left panel) and *hisΔHC-Pro* (right panel). Purified protein solutions were (+) or were not (-) subjected to cross-linking and analyzed by Coomassie Blue staining after SDS-PAGE.

pected by random combination of the two subforms of *hisΔHC-Pro*. This might have been because of the poor resolution of the SDS-PAGE gels for high molecular mass proteins.

HC-Pro Contains a Protease-resistant Domain—We carried out limited tryptic proteolysis of purified *hisHC-Pro* and *hisΔHC-Pro*. Fig. 4*A* shows that trypsin degraded *hisHC-Pro* to a 32-kDa peptide. This peptide was very resistant to prolonged proteolysis. Trypsin digestion of *hisΔHC-Pro* (Fig. 4*A*) also yielded a 32-kDa peptide. This indicated that the 32-kDa peptide originated from the middle or C-terminal part of the entire *hisHC-Pro* molecule. N-terminal sequencing of the 32-kDa peptides showed that both *hisHC-Pro* and *hisΔHC-Pro* were cleaved at AA Thr¹⁷⁰ or Gly¹⁷⁶ (numbering according to wild-type HC-Pro) suggesting that this stretch of the HC-Pro molecule is exposed. Chemical cross-linking of the 32-kDa peptide of *hisHC-Pro* and *hisΔHC-Pro* with glutaraldehyde revealed that the region sufficient for dimerization is contained in the C-terminal 282 AA of HC-Pro (Fig. 4*B*). Tetramers and higher oligomeric forms of HC-Pro were also observed as with full-length HC-Pro and Δ HC-Pro. Chemical cross-linking experiments with Src homology-reactive and lysine-reactive compounds gave similar results (data not shown).

2D Crystallization of *hisHC-Pro* and *hisΔHC-Pro*—2D crystallization of *hisHC-Pro* and *hisΔHC-Pro* was achieved after binding onto a lipid monolayer. The nickel-chelating lipid used in this study was 1,2-dioleoyl-sn-glycero-3-[(*N*-(5-amino-1-carboxypentyl)imidodiacetic acid)succinyl] (nickel salt) (DOGS-Ni-NTA). A systematic screening of crystallization conditions revealed that Mg²⁺ in the buffer was crucial to induce crystallization of both recombinant proteins. *hisHC-Pro* crystals were extremely fragile and most often broke when transferred onto plain carbon grids. Subsequently, 2D crystals were transferred onto holey carbon grids and then carbon-coated (27).

Fig. 5, *A* and *B* shows typical *hisHC-Pro* and *hisΔHC-Pro* 2D crystals. They had well defined edges forming step-like structures. *hisHC-Pro* formed large 2D crystals with 1 to 10 μ m in diameter containing many defects when examined at higher magnification. Fig. 5, *C* and *D* show a representation of the Fourier components determined from a single image. The quality of *hisΔHC-Pro* crystals was clearly better than that of *hisHC-Pro* crystals. Indeed, for *hisΔHC-Pro* crystals, reliable factors up to

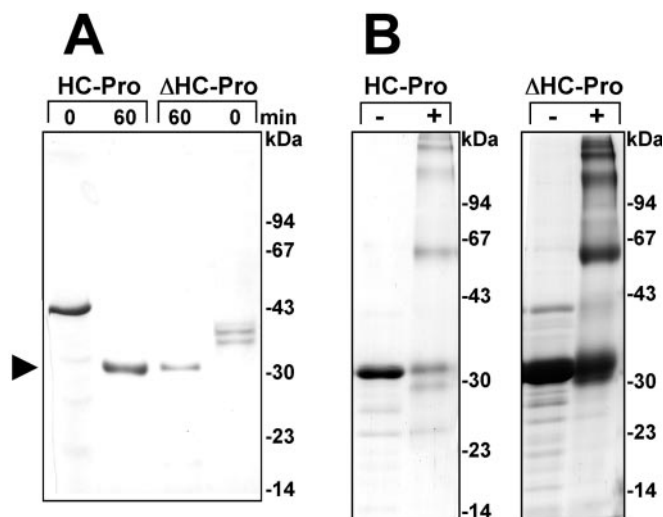


FIG. 4. *hisHC-Pro* and *hisΔHC-Pro* contain a trypsin-resistant dimerization domain. *A*, purified *hisHC-Pro* (first two lanes) and *hisΔHC-Pro* (next two lanes) were incubated with trypsin for the times indicated, and digestion products were analyzed by Coomassie Blue staining after SDS-PAGE. The 32-kDa peptide (arrowhead) was readily detectable even after prolonged digestion (not shown). *B*, the 32-kDa peptide released by trypsin digestion is cross-linked by glutaraldehyde to a dimer. The panels show Coomassie Blue-stained gels after SDS-PAGE of trypsin digests of *hisHC-Pro* (left panel) and *hisΔHC-Pro* (right panel) that were (+) or were not (-) subjected to cross-linking after trypsin digestion. Note that additional cross-linked products corresponding to a tetramer of the 32-kDa peptide were visible.

17-Å resolution were visible in the optical diffraction pattern whereas the upper limit resolution obtained from *hisHC-Pro* crystals was usually comprised between 25 and 20 Å.

The unit cell parameters determined from averaged images are presented in Table I. Although the molecular mass of *hisΔHC-Pro* is 22% smaller than that of *hisHC-Pro*, its unit cell is 12% larger. This certainly reflects different protein packing of *hisΔHC-Pro* in the crystal. Examination of the phase relationships indicated a *p4* plane group for both 2D crystals (32).

Projection Maps Calculated from Negatively Stained 2D Crystals Reveal Two Structural Domains—Images of crystals were recorded as described under “Materials and Methods.” An inherent problem of using holey carbon grids to pick up crystals at the interface of the crystallizing wells is that most recorded images derive from more or less randomly tilted 2D crystals. Merging such images leads to blurred projection maps. Thus, for a better understanding, we present projection maps calculated from single images. To better compare the projection maps, a resolution cut-off at 23 Å was applied to images of the two proteins before calculation of the final projection maps (Fig. 6).

The *hisHC-Pro* density map presented in Fig. 6*A* revealed a tetrameric organization of the protein. The tetramer has a square-like shape with \sim 78-Å side length. The unit cell contains one tetramer and is presented by a *black square box* in Fig. 6*A*. The smaller repeat unit delimited in *black* shows an elongated form with a length of 54 Å and is composed of two domains, designated 1 and 2, of \sim 26 and 22 Å in diameter, respectively. Domain 1 is located close to the center of the tetramer and connected to domain 2 by a constriction. Four domains 2 form the corners of the tetramer. The *hisHC-Pro* monomer has been assigned to the domains 1 plus 2, based on comparison with projection maps of other soluble proteins (41, 42) and taking into account the hypothetical surface *hisHC-Pro* would occupy with an overall bi-lobular shape.

The projection map calculated from negatively stained 2D crystals of *hisΔHC-Pro* was quite different and revealed an

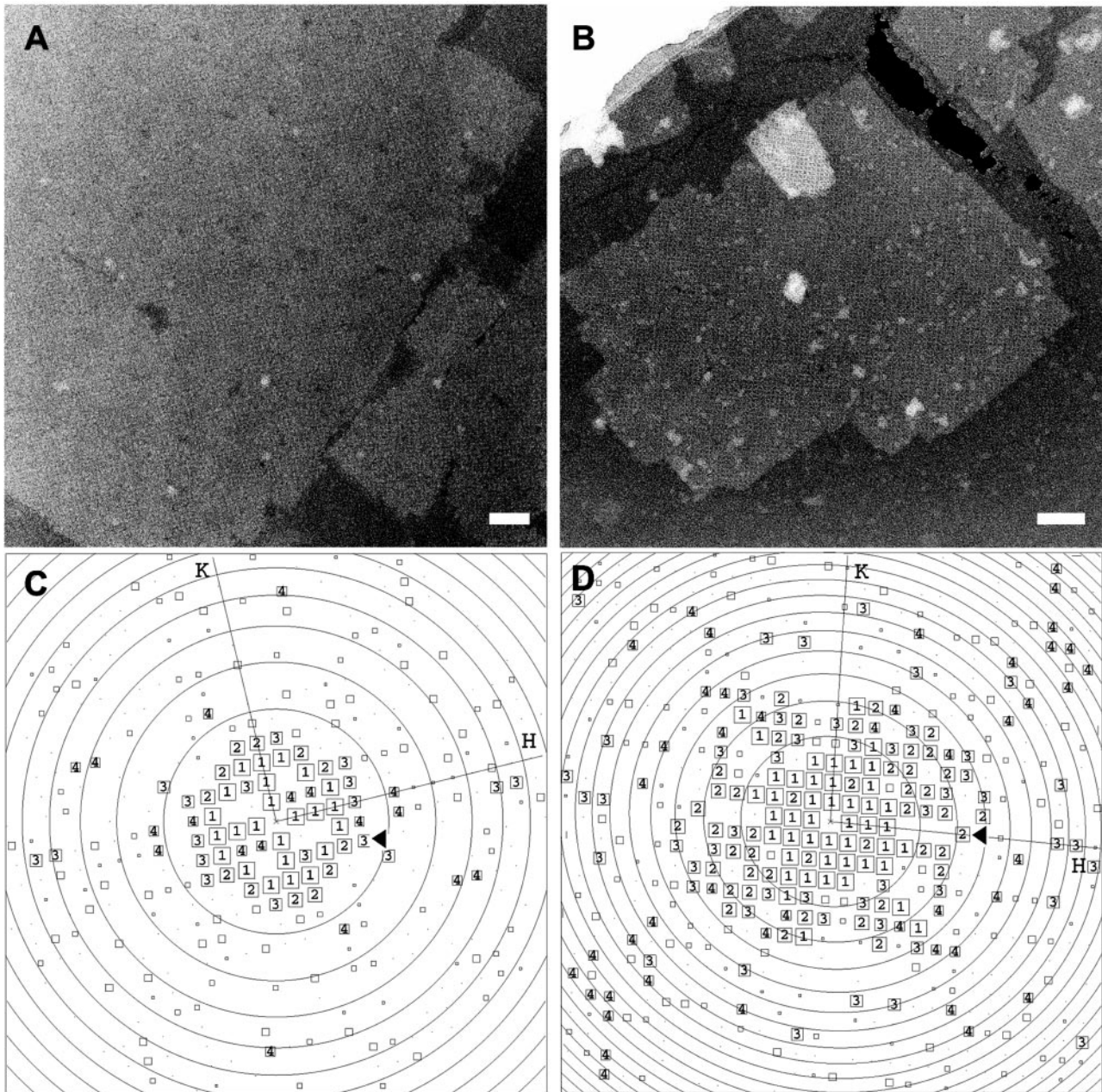


FIG. 5. Two-dimensional crystals of hisHC-Pro and his Δ HC-Pro. Electron micrographs of negatively stained 2D crystals of hisHC-Pro (A) and his Δ HC-Pro (B) were recorded using a Philips CM12 electron microscope at a magnification of $\times 43,750$. 2D crystals grew on lipid monolayers consisting of Ni-NTA DOGS/dioleoyl phosphatidylcholine at a molar ratio of 1/1. Scale bars correspond to 100 nm. C and D, show the Fourier components calculated from images A and B. Concentric lines indicate the zero values of the phase-contrast transfer function for a defocus of 8726 and 14473 Å, respectively. H and K axes refer to the reciprocal lattice vectors. Each box represents a reflection, and the size and the number within it (IQ values) relate to the quality of the data. A low IQ value reflects a high signal-to-noise ratio (30, 31). Black arrows in C and D indicate a resolution of 21.7 and 14.6 Å, respectively.

altered crystal packing (Fig. 6B). Two types of tetrameric motifs are observed in the projection map, located at the corner and in the center of the unit cell, respectively. They overlap and show a mesh-like organization (Fig. 6B). The smaller, elongated repeat unit *encircled in black* has a length of 57 Å and consists, like hisHC-Pro, of two globular domains of 26 and 22 Å in diameter, respectively. These domains were accordingly termed 1' and 2'. Four domains 1' form the tetrameric structure located at the corners of the unit cell while the tetrameric structure present into the center of the unit cell results from merging of four domains 2'.

A comparison of the projection maps is presented in Fig. 7. The hisHC-Pro tetramer was not simply superimposable on the his Δ HC-Pro tetramer. Instead, a rotation of the entire hisHC-

Pro tetramer by 4° was required to superimpose domains 1 and 1'. In addition, two further operations (rotation by 26° and shift of 3 Å of domain 2) were necessary to superimpose domains 2 and 2'. These geometric operations suggest that the two domains are separated by a flexible region and are probably structurally independent. Structural modifications in his Δ HC-Pro induced more contacts between domains 2', strengthening crystal stability and providing an explanation for the better quality of these crystals. Because hisHC-Pro and his Δ HC-Pro monomers were not directly superimposable, we computed average profiles of the two monomers to determine location of the domains in the HC-Pro sequence (Fig. 7B). Negative staining provides information about stain exclusion domains, and a loss of density in a domain could be linked to a loss of volume.

TABLE I
Crystallographic data

Negative stain	HC-Pro	Δ HC-Pro
Plane group symmetry	$P4$	$P4$
Unit cell parameters	$a = 95.6 \pm 0.6 \text{ \AA}$ $b = 94.5 \pm 0.9 \text{ \AA}$ $\gamma = 90.3 \pm 1.4^\circ$	$a = 101.9 \pm 1.1 \text{ \AA}$ $b = 99.5 \pm 2.2 \text{ \AA}$ $\gamma = 89.3 \pm 2.5^\circ$
Cryo		
Number of images	4	
Plane group symmetry	$P4$	
Unit cell parameters	$a = 103.0 \pm 0.2 \text{ \AA}$ $b = 102.9 \pm 0.3 \text{ \AA}$ $\gamma = 90.0 \pm 0.3^\circ$	
Resolution range in \AA	Number of unique reflections	Phase residual (deg.) compared with $0^\circ/180^\circ$ with IQ 5 maximum (45° is random)
300.0–17.4	28	17.7
17.4–12.2	26	23.4
12.2–10.0	27	25.3
10.0–8.6	20	34.9
Total range 300–8.6	101	24.6

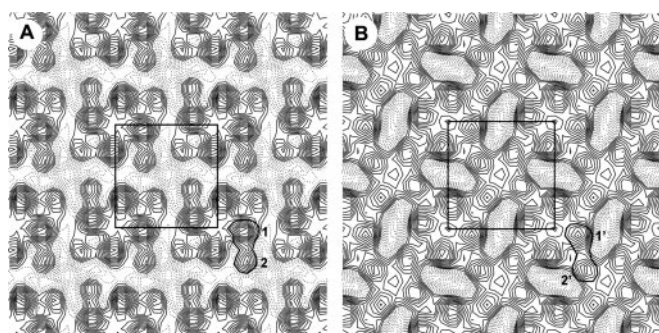


FIG. 6. Projection map of negative-stained 2D crystals of hisHC-Pro and his Δ HC-Pro. A, projection map of hisHC-Pro. A hisHC-Pro monomer, encircled in black, is composed of two structural domains named 1 and 2, of 26 and 22 Å in diameter, respectively. Total length of the monomer is 54 Å. B, projection map of his Δ HC-Pro. The crystal packing involves more intermolecular contacts. The monomer is composed of two structural domains labeled 1' and 2' with 26 and 22 Å in diameter. his Δ HC-Pro is 57 Å long. Four adjacent domains 2' form the tetramer present in the middle of the unit cell. Maps were calculated from a single image, and no symmetry operation was imposed. A resolution cut off of 23 Å was applied before computing the maps. The unit cells are presented by a black square box; for hisHC-Pro $a = 96 \text{ \AA}$, $b = 95 \text{ \AA}$, $\gamma = 90^\circ$; for his Δ HC-Pro $a = 102 \text{ \AA}$, $b = 100 \text{ \AA}$, $\gamma = 89^\circ$.

his Δ HC-Pro showed a density decrease in domain 1', suggesting that the N terminus is located in domain 1 of hisHC-Pro.

Cryo-microscopy of his Δ HC-Pro—2D crystals of his Δ HC-Pro, being of higher quality than those of hisHC-Pro, were used for further investigation by cryo-microscopy. Fig. 8A shows a typical computed transform with reliable reflections up to 8-Å resolution. The images clearly identify a tetragonal unit cell with $a = b = 103 \text{ \AA}$. Examination of the phase relationships indicated a $p4$ plane group (32) as found for negatively stained crystals. Four images were analyzed and combined to generate a data set of 101 averaged reflections up to 8.6-Å resolution. After refinement to 0 or 180°, the overall phase residual up to 8.6-Å resolution was 24.6° (45° would be random), indicating that all symmetry-related reflections were reliable (Table I). A fully symmetrized projection map at 9-Å resolution is presented in Fig. 8B. In this projection structure, the molecular boundaries of the his Δ HC-Pro monomer are now more clearly resolved and delimited in black in Fig. 8B. his Δ HC-Pro has a length of 63 Å and is composed of two domains as in the negatively stained projection map. Domain 1' has a square-like

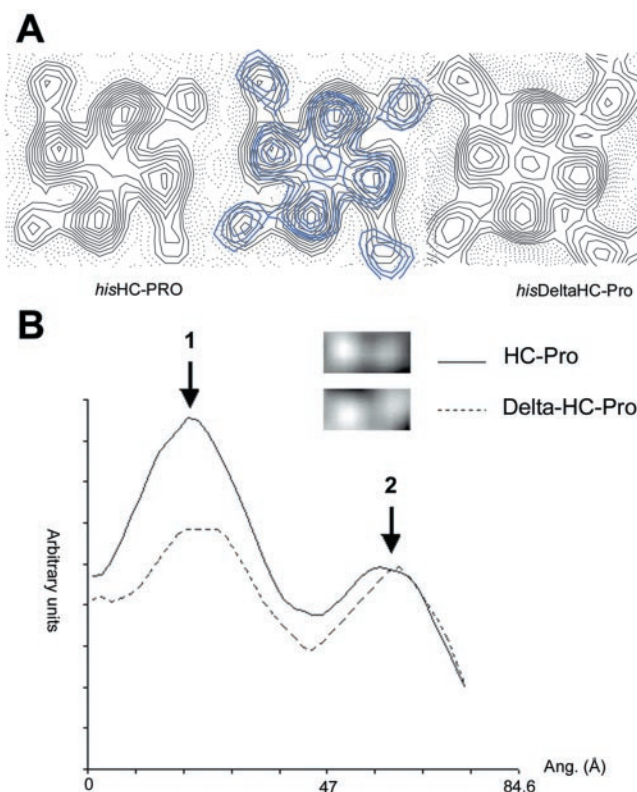


FIG. 7. Comparison of projection maps from negative-stained 2D crystals. A, the hisHC-Pro and his Δ HC-Pro tetramers shown were extracted from projection maps of negatively stained crystals. The middle inset displays superposition of his Δ HC-Pro (in blue) and hisHC-Pro. A rotation of 4° of the whole his Δ HC-Pro tetramer is required to superimpose domains 1 and 1'. Two additional geometric operations are needed to superimpose domains 2 and 2', a rotation of 26° plus a shift of 3 Å. B, hisHC-Pro and his Δ HC-Pro averaged profiles. Profiles were normalized to be comparable. 1 and 2 above the curves refer to structural domains. The 99-AA deletion in his Δ HC-Pro results in a density decrease in domain 1'.

shape with 27-Å side length and is connected to domain 2' by a constriction of roughly 16-Å diameter. Domain 2' has a rectangular shape with 27 Å in length and 22 Å in width. Variation in measurements with those obtained from negatively stained crystal projection maps likely resulted from the stain drying process. The map reflects the projected electron density of the protein and subsequently is directly related to its mass. Thus, the whole density of his Δ HC-Pro corresponds to a molecular mass of 41,325 Da. Domains 1' and 2' represent 63 and 37% of the density, corresponding to masses of about 26 and 15 kDa and consecutively to about 228 and 139 AA. New structural features are clearly resolved in the projection map, in particular high density peaks are seen in domains 1' and 2'. These peaks have a round shape of 10 to 15 Å in diameter and might be related to projection of α -helices (42, 43).

Predictions of the Secondary Structures Suggest Two Structural Domains—Prediction of the secondary structure of hisHC-Pro was carried out using different programs. All these programs gave similar results. Fig. 9A presents the results obtained with the Hnn program (35). Two helix-rich regions (AA 40–235 and AA 330–458) connected by a less structured region of about 95 AA are predicted (Fig. 9B). This suggests that HC-Pro is composed of two compact domains connected by a less structured domain. This assumption correlates strongly with our experimental results, notably with the projection map obtained from frozen-hydrated his Δ HC-Pro 2D crystals. We showed that the N terminus is located in the larger domain of HC-Pro, i.e. domain 1. This correlates well with the first pre-

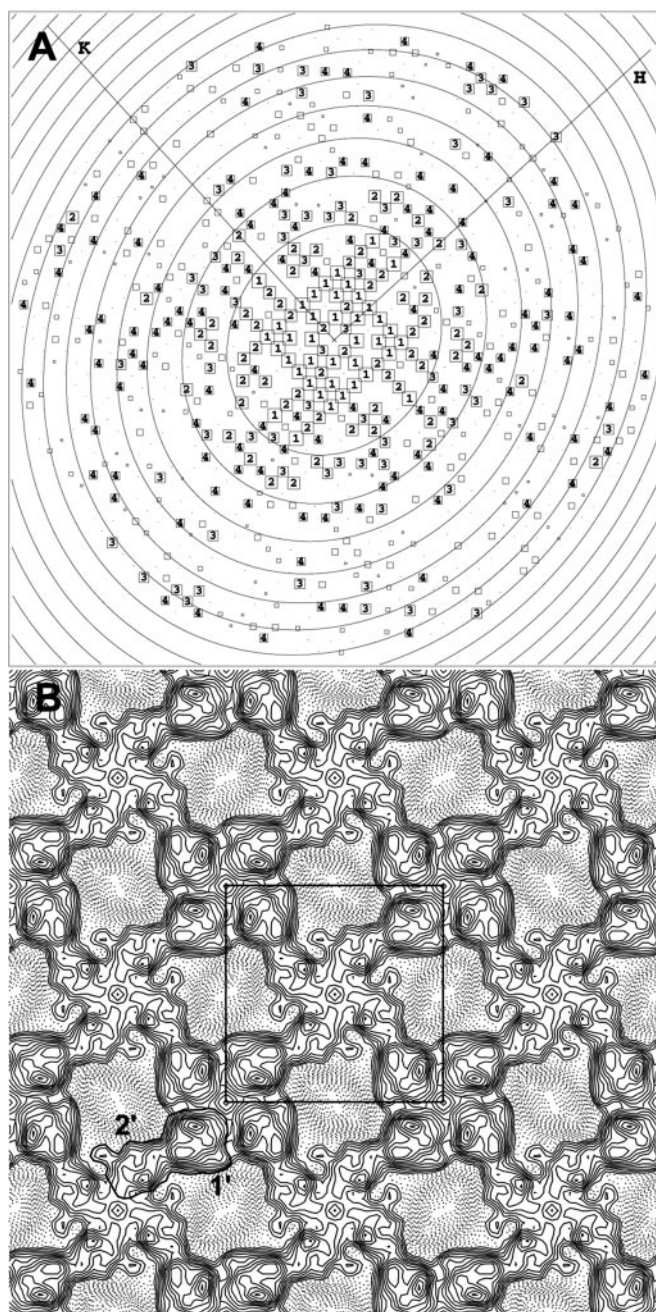


FIG. 8. Projection structure of frozen-hydrated 2D crystals of *his*ΔHC-Pro. A, Fourier components calculated from a single image of a *his*ΔHC-Pro 2D crystal. The edge of the plot corresponds to a resolution of 5 Å. The axes refer to the reciprocal lattice vectors. B, projection map of *his*ΔHC-Pro. The projection density map with $p4$ symmetry imposed was calculated to 9-Å resolution using amplitudes and phases from four images. One unit cell with $a = 103$ Å, $b = 103$ Å and a *his*ΔHC-Pro monomer are outlined in black. The zero-level was derived from the mean density of the map.

dicted helix-rich domain located at the N-terminal extremity. We conclude that the HC-Pro structure determined here is closely related to the predicted secondary structure, the two helix-rich regions, and the less structured region corresponding to structural domains 1 and 2 and the hinge domain, respectively.

DISCUSSION

The main goal of this study was to provide information on structure of the potyviral multifunctional protein HC-Pro to relate structure with biological functions. Three-dimensional

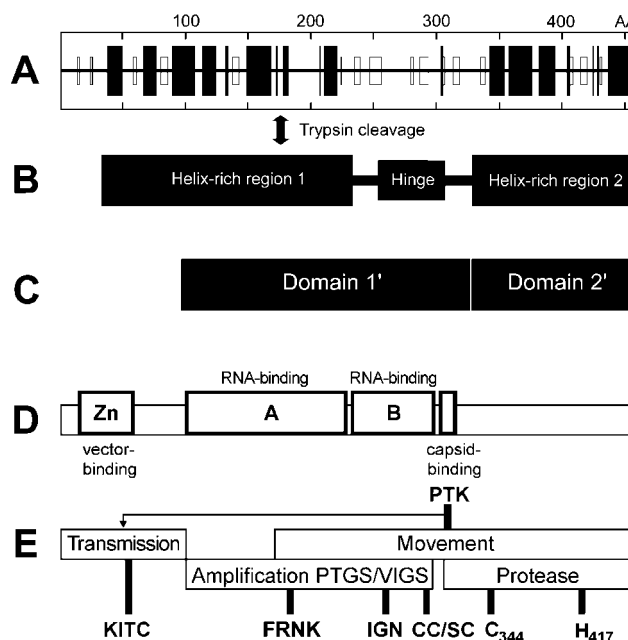


FIG. 9. Alignment of structural domains, predicted helices, and biological functions of HC-Pro. A, HC-Pro secondary structure as predicted by the Hnn program. Black boxes represent regions with high α -helix probability, and open boxes represent regions with high β -sheet probability. B, schematic drawing of the regions covering the suggested two helix-rich regions that are separated by a less structured hinge region. Limits of these domains correspond to the average limits obtained from the different predictive methods. The arrow indicates the trypsin cleavage sites at AA 170 and 176. C, position of structural domains 1' and 2' of *his*ΔHC-Pro with the assumption that structural domains and sequence are linearly correlated. D and E, same as in Fig. 1.

crystallization trials not being successful, we decided to elucidate the structure of HC-Pro by biochemistry, electron microscopy, and image analysis.

Earlier work by Thornbury *et al.* (3) and Wang and Pirone (20) demonstrated that the HC-Pro of *Tobacco vein mottling virus*, *Potato virus Y*, and *Turnip mosaic virus* behave like dimers or trimers in size exclusion chromatography. We confirmed these data for the LMV *his*HC-Pro and suggest that this could be a general feature of potyviral HC-Pro molecules. We were unable to discern the exact oligomerization state of soluble HC-Pro from our chromatography results. However, in chemical cross-linking experiments, *his*HC-Pro reaction products appeared with a mass corresponding to a dimer but never to a trimer. Our data thus strongly suggest that soluble HC-Pro is a dimer and that the aberrant elution behavior of HC-Pro in gel filtration is probably caused by its elongated shape. Structural characterization of HC-Pro by electron microscopy confirms these assumptions.

We successfully grew 2D crystals of the two recombinant proteins on lipid monolayers containing Ni-NTA (23, 44). Crystallization occurred only in the presence of Mg^{2+} . This cation has been shown previously (45) to increase potyviral transmission rate in *in vitro* assays where aphids were fed crude or partially purified HC-Pro-containing extracts from infected plants. Our own observation reported here possibly indicates that Mg^{2+} has an unknown organizing and/or stabilizing effect on the HC-Pro molecule.

Both recombinant proteins crystallized with $p4$ symmetry. It is quite surprising to obtain a $p4$ plane group symmetry, because we demonstrated previously that HC-Pro has a dimeric behavior in solution. Our observations² suggest that *his*HC-Pro

² P. Bron, unpublished data.

and *his* Δ HC-Pro first interacted with the lipid monolayer as dimers and then started to form dimers of dimers resulting in a tetrameric state. Unfortunately, at this stage, we cannot conclude on the structural organization of the HC-Pro dimer in solution.

The analysis performed with negatively stained 2D crystals showed that both *his*HC-Pro and *his* Δ HC-Pro have an elongated shape and are composed of two structural domains. Comparison of projection maps allowed us to conclude that the two structural domains are connected by a flexible region and that the N terminus is located in domain 1. The fact that domains 1 and 1' of the two proteins have equivalent diameters suggests that the domain formed by the first 102 N-terminal AA in *his*HC-Pro is located in the perpendicular plane of the crystal. Although lacking 22% of the mass of the wild-type protein, *his* Δ HC-Pro is still organized as a tetramer in the crystal. These observations suggest that the N-terminal 102 AA do not interfere strongly with the rest of the molecule and are likely structurally isolated. This could be confirmed by comparing three-dimensional models of *his*HC-Pro and *his* Δ HC-Pro.

Several reports (21, 22, 46) suggested that the cysteine-rich region located in the N-terminal region of HC-Pro might contain a self-interaction domain because of its homology with Zn-finger-like motifs (47). Although we do not rule out that this region is capable of self-interaction or interaction with other molecules, we present here convincing evidence that this region is not essential for dimerization or functions other than transmission. First, symptoms caused by the LMV mutant harboring *his* Δ HC-Pro were indistinguishable from those induced by the wild-type virus, indicating that all functions required for infection are located downstream of the deletion. Second, properties of *his* Δ HC-Pro in size exclusion chromatography, cross-linking, and crystallization were very similar to *his*HC-Pro. The *his*HC-Pro projection map shows that the tetrameric organization results from interactions of domains 1, which contain the N-terminal extremity. However, intermolecular contacts between domain 2 and domain 1 were also observed. In *his* Δ HC-Pro projection structures, the tetrameric organization is conserved and results from similar interactions. The only possible conclusion of these results is that the N-terminal 102 AA of HC-Pro are not essential for dimerization and that an essential self-interaction domain is located in the remaining part of the molecule. Finally, cross-linking studies with a 32-kDa trypsin digestion product of *his*HC-Pro further delineated a dimerization domain to the C-terminal 282 AA. This is consistent with the results from Guo *et al.* (22) who identified a HC-Pro self-interaction domain in the C-terminal ~130 AA of HC-Pro by yeast double-hybrid assay.

Predictions of the secondary structures of HC-Pro are consistent with our results, notably with the projection structure at 9-Å resolution of frozen-hydrated *his* Δ HC-Pro. This suggests a linear correlation between structural domains identified in projection maps and domains predicted from the amino acid sequence analysis (Fig. 9). Combined together, the results enable us to propose a structure/function model for HC-Pro. HC-Pro is elongated and composed of different structural domains. We propose that the proteinase activity mapped previously (4) to the C-terminal 155 AA corresponds to structural domain 2'. The structural domain 1, rich in α -helices, contains the hinge at its C-terminal extremity. The hinge region, suggested by secondary structure prediction and identified in the projection maps as a constriction between domains 1 and 2, was remarkably resistant to trypsin digestion, implying that it is probably well structured. Prediction programs indicate that this region is composed mainly of β -sheets. This structural organization does not rule out the small dislocation of the two domains as

observed from comparison of *his*HC-Pro and *his* Δ HC-Pro projection maps. The ~90 AA comprising this region overlap well with RNA binding domain B (15) and contain important conserved motifs like IGN, CC/SC, and PTK. Thus, this section of HC-Pro is most probably more than just a hinge but presents a domain of its own. Functionally, it is associated with virus movement, genome amplification, RNA silencing, and coat protein binding. The N-terminal extremity of the structural domain 1' corresponds to the helix-rich region 1 minus the first 99 AA. The region comprising AA 170–176 is probably exposed and not structured. This is shown by susceptibility of this region to trypsin digestion, resulting in fast degradation of the entire N terminus. It is interesting to note that the highly conserved FRNK motif is just downstream of AA 176. Likely, structure or location shielded this box from trypsin digestion, because it was not degraded although it contains potential trypsin cleavage sites. This part (AA 100–225) of helix-rich region 1 corresponds to the RNA binding site A identified previously (15) and functionally contains parts of the regions involved in viral movement, genome amplification, and RNA silencing. As mentioned above, although helix-rich region 1 stretches from AA 1 to 275, the first 102 AA should be structurally isolated from the rest of the molecule, because its deletion does not modify the projection structure of the molecule in negative staining.

In conclusion, we establish here the first basis to relate structure of HC-Pro with its multifunctional roles. It is interesting to observe that all functions of HC-Pro, except the self-cleavage function that is fully contained in domain 2, involve more than one structural domain. The transmission function needs the N terminus and the PTK motif in the hinge domain. RNA silencing, virus movement, and genome amplification are associated with domain 1 and the hinge domain. The latter functions were suggested to be closely related (19). Whether this implies that they use the same active sites in domain 1 and the hinge, that different sites or combinations of sites in the same region are used, or that different host or viral interaction partners compete with the same sites for different functions, remains to be determined. We here hypothesize that domain 1 contains the active sites needed for the various functions and that the hinge domain regulates their accessibility by moving domain 2 to mask or expose domain 1. The movement of the hinge domain could, in turn, be regulated by interaction with various host or viral partners.

Acknowledgments—We thank Denis Chretien, Cyrille Garnier, and Isabelle Arnal for critical reading of the manuscript. We gratefully acknowledge Dr. D. Levy for helpful discussions on the 2D crystallization. Thanks to Hervé LeCoq for HC-Pro antiserum, Pascal Espérandieu for gardening, and Jean Derancourt for help with protein sequencing.

REFERENCES

- Raccah, B., Huet, H., and Blanc, S. (2001) in *Virus-Insect-Plant Interactions* (Harris, K., Duffus, J. E., and Smith, O. P., eds) pp. 181–206, Academic Press, San Diego, CA
- Urcuqui-Inchima, S., Haenni, A. L., and Bernardi, F. (2001) *Virus Res.* **74**, 157–175
- Thornbury, D. W., Hellman, G. M., Rhoads, R. E., and Pirone, T. P. (1985) *Virology* **144**, 260–267
- Oh, C. S., and Carrington, J. C. (1989) *Virology* **173**, 692–699
- Kasschau, K. D., Cronin, S., and Carrington, J. C. (1997) *Virology* **228**, 251–262
- Anandalakshmi, R., Pruss, G. J., Ge, X., Marathe, R., Mallory, A. C., Smith, T. H., and Vance, V. B. (1998) *Proc. Natl. Acad. Sci. U.S.A.* **95**, 13079–13084
- Blanc, S., Ammar, E. D., Garcia-Lampasona, S., Dolja, V. V., Llave, C., Baker, J., and Pirone, T. P. (1998) *J. Gen. Virol.* **79**, 3119–3122
- Blanc, S., Lopez-Moya, J. J., Wang, R., Garcia-Lampasona, S., Thornbury, D. W., and Pirone, T. P. (1997) *Virology* **231**, 141–147
- Peng, Y. H., Kadoury, D., Gal-On, A., Huet, H., Wang, Y., and Raccah, B. (1998) *J. Gen. Virol.* **79**, 897–904
- Roudet-Tavert, G., German-Retana, S., Delaunay, T., Delecote, B., Candresse, T., and Le Gall, O. (2002) *J. Gen. Virol.* **83**, 1765–1770

11. Dolja, V. V., Herndon, K. L., Pirone, T. P., and Carrington, J. C. (1993) *J. Virol.* **67**, 5968–5975
12. Rojas, M. R., Zerbini, F. M., Allison, R. F., Gilbertson, R. L., and Lucas, W. J. (1997) *Virology* **237**, 283–295
13. Cronin, S., Verchot, J., Haldeman-Cahill, R., Schaad, M. C., and Carrington, J. C. (1995) *Plant Cell* **7**, 549–559
14. Maia, I. G., and Bernardi, F. (1996) *J. Gen. Virol.* **77**, 869–877
15. Urcuqui-Inchima, S., Maia, I. G., Arruda, P., Haenni, A. L., and Bernardi, F. (2000) *Virology* **268**, 104–111
16. Voinnet, O. (2001) *Trends Genet.* **17**, 449–459
17. Wan, X. L., and Ding, S. W. (2001) *Curr. Opin. Biotechnol.* **12**, 150–154
18. Mallory, A. C., Ely, L., Smith, T. H., Marathe, R., Anandalakshmi, R., Fagard, M., Vaucheret, H., Pruss, G., Bowman, L., and Vance, V. B. (2001) *Plant Cell* **13**, 571–583
19. Kasschau, K. D., and Carrington, J. C. (2001) *Virology* **285**, 71–81
20. Wang, R. Y., and Pirone, T. P. (1999) *Phytopathology* **89**, 564–567
21. Urcuqui-Inchima, S., Walter, J., Drugeon, G., German-Retana, S., Haenni, A. L., Candresse, T., Bernardi, F., and Le Gall, O. (1999) *Virology* **258**, 95–99
22. Guo, D., Merits, A., and Saarma, M. (1999) *J. Gen. Virol.* **80**, 1127–1131
23. Kornberg, R. D., and Darst, S. A. (1991) *Curr. Opin. Struct. Biol.* **1**, 642–646
24. Yang, S. J., Revers, F., Souche, S., Lot, H., Le Gall, O., Candresse, T., and Dunez, J. (1998) *Arch. Virol.* **143**, 2443–2451
25. German-Retana, S., Candresse, T., Alias, E., Delbos, R. P., and Le Gall, O. (2000) *Mol. Plant-Microbe Interact.* **13**, 316–324
26. Levy, D., Mosser, G., Lambert, O., Moeck, G. S., Bald, D., and Rigaud, J. L. (1999) *J. Struct. Biol.* **127**, 44–52
27. Brisson, A., Bergsma-Shutter, W., Oling, F., Lambert, O., and Reviakine, I. (1999) *J. Growth Cryst.* **196**, 456–470
28. Dubochet, J., Adrian, M., Chang, J. J., Homo, J. C., Lepault, J., McDowell, A. W., and Schultz, P. (1988) *Q. Rev. Biophys.* **21**, 129–228
29. Crowther, R. A., Henderson, R., and Smith, J. M. (1996) *J. Struct. Biol.* **116**, 9–16
30. Henderson, R., Baldwin, J. M., Downing, K. H., Lepault, J., and Zemlin, F. (1986) *Ultramicroscopy* **19**, 147–178
31. Henderson, R., Baldwin, J. M., Ceska, T. A., Zemlin, F., Beckmann, E., and Downing, K. H. (1990) *J. Mol. Biol.* **213**, 899–929
32. Valpuesta, J. M., Carrascosa, J. L., and Henderson, R. (1994) *J. Mol. Biol.* **240**, 281–287
33. Collaborative Computational Project Number 4 (1994) *Acta Crystallogr. Sect. D Biol. Crystallogr.* **50**, 760–763
34. Rost, B., Sander, C., and Schneider, R. (1994) *Comput. Appl. Biosci.* **10**, 53–60
35. Combet, C., Blanchet, C., Geourjon, C., and Deleage, G. (2000) *Trends Biochem. Sci.* **25**, 147–150
36. Kneller, D. G., Cohen, F. E., and Langridge, R. (1990) *J. Mol. Biol.* **214**, 171–182
37. McClelland, J. L., and Rumelhart, D. E. (1988) *Explorations in Parallel Distributed Processing*, Vol. 3, pp. 318–362, MIT Press, Cambridge, MA
38. Cuff, J. A., and Barton, G. J. (2000) *Proteins* **40**, 502–511
39. Cuff, J. A., Clamp, M. E., Siddiqui, A. S., Finlay, M., and Barton, G. J. (1998) *Bioinformatics* **14**, 892–893
40. Geourjon, C., and Deleage, G. (1995) *Comput. Appl. Biosci.* **11**, 681–684
41. Venien-Bryan, C., Balavoine, F., Toussaint, B., Mioskowski, C., Hewat, E. A., Helme, B., and Vignais, P. M. (1997) *J. Mol. Biol.* **274**, 687–692
42. Venien-Bryan, C., Schertler, G. F., Thouvenin, E., and Courty, S. (2000) *J. Mol. Biol.* **296**, 863–871
43. Bron, P., Lacapere, J. J., Breyton, C., and Mosser, G. (1999) *J. Mol. Biol.* **287**, 117–126
44. Uzgiris, E. E., and Kornberg, R. D. (1983) *Nature* **301**, 125–129
45. Govier, D. A., Kassanis, B., and Pirone, T. P. (1977) *Virology* **78**, 306–314
46. Urcuqui-Inchima, S., Maia, I. G., Drugeon, G., Haenni, A. L., and Bernardi, F. (1999) *J. Gen. Virol.* **80**, 2809–2812
47. Robaglia, C., Durand-Tardif, M., Tronchet, M., Boudazin, G., Astier-Manificier, S., and Casse-Delbart, F. (1989) *J. Gen. Virol.* **70**, 935–947